

Effect of membrane deformation on performance of vacuum assisted air gap membrane distillation (V-AGMD)

Yusik Kim¹, Jihyeok Choi¹, Yongjun Choi¹ and Sangho Lee^{*1,2}

¹School of Civil and Environmental Engineering, Kookmin University, 77 Jeongneung-ro, Seongbuk-Gu, Seoul, 02707, Republic of Korea

²Desalination Technologies Research Institute (DTRI), Saline Water Conversion Corporation (SWCC), WQ36+XJP, Al Jubayl 35417, Kingdom of Saudi Arabia

(Received June 20, 2021, Revised September 6, 2021, Accepted September 28, 2021)

Abstract. Vacuum-assisted air gap membrane distillation (V-AGMD) has the potential to achieve higher flux and productivity than conventional air gap membrane distillation (AGMD). Nevertheless, there is not much information on technical aspects of V-AGMD operation. Accordingly, this study aims to analyze the effect of membrane deformation on flux in V-AGMD operation. Experiments were carried out using a bench-scale V-AGMD system. Statistical models were applied to understand the flux behaviors. Statistical models based on MLR, GNN, and MLFNN techniques were developed to describe the experimental data. Results showed that the flux increased by up to 4 times with the application of vacuum in V-AGMD compared with conventional AGMD. The flux in both AGMD and V-AGMD is affected by the difference between the air gap pressure and the saturation pressure of water vapor, but their dependences were different. In V-AGMD, the membranes were found to be deformed due to the vacuum pressure because they were not fully supported by the spacer. As a result, the deformation reduced the effective air gap width. Nevertheless, the rejection and LEP were not changed even if the deformation occurred. The flux behaviors in V-AGMD were successfully interpreted by the GNN and MLFNN models. According to the model calculations, the relative impact of the membrane deformation ranges from 10.3% to 16.1%.

Keywords: air gap membrane distillation (AGMD); artificial neural network; flux; membrane deformation; vacuum; vacuum-assisted AGMD (V-AGMD)

1. Introduction

Water shortage is continuously increasing due to the growth of population, development of urban areas, and advances in industrial sectors (Ahmed *et al.* 2020). Uncertainty in water resource availability is also increasing due to climate change (Kundzewicz *et al.* 2018). Inadequate water supply imposes a threat to the sustainability of the economic and social development (Dolan *et al.* 2021). Accordingly, it is inevitable to explore ways to alleviate water scarcity by securing alternative water resources (Choi *et al.* 2020, Aziz and Hanafiah 2021). Desalination has been accepted as a promising method to provide an ongoing supply of freshwater by removing salts from seawater or brackish water (Pinto and Marques 2017, Hamdan *et al.* 2021). Currently, desalination covers nearly 1% of the global water supply but its market is predicted to grow at 8% between 2018 and 2025 (Ahmed *et al.* 2020, Caldera and Breyer 2020, Zhao *et al.* 2021).

There are two types of desalination processes, including thermally driven technology and pressure-driven technology (Qasim *et al.* 2019). The first type includes multi-stage flash (MSF), multi-effect distillation (MED), and humidification-dehumidification processes (Ali *et al.* 2018). The second type includes reverse osmosis (RO)

membrane processes (Atab *et al.* 2016). Due to many advantages, including ease of operation, compactness, reduction in chemical usages, and relatively low energy consumption, RO is becoming a preferred desalination technique (Pinto and Marques 2017, Goh *et al.* 2018). Nevertheless, RO still has many technical issues including the production and discharge of high-salinity brines (Missimer and Maliva 2018, Pistocchi *et al.* 2020, Ihsanullah *et al.* 2021, Zhao *et al.* 2021). Since the adverse impacts of brine discharge into sea rise increasing concerns, it is necessary to develop novel technologies to reduce brine production by increasing the recovery of the product water (Altaee *et al.* 2014, Lee *et al.* 2019). Unfortunately, the permeate recovery in RO is restricted by the osmotic pressure of the brine (Kim *et al.* 2019, Lee *et al.* 2019).

Among various technological options to reduce the generation of brine, membrane distillation (MD) has been extensively considered (Alkhudhiri *et al.* 2012, Drioli *et al.* 2015, Thomas *et al.* 2017, Alsebaei and Ahmad 2020, Skuse *et al.* 2021). Unlike RO, MD is a separation technique utilizing thermal energy and can be operated at a high recovery of product water (Alkhudhiri *et al.* 2012, González *et al.* 2017, Alsebaei and Ahmad 2020, Jiang *et al.* 2021). Thus, the volume of brine generated by MD brine may be smaller than that by RO (Ruiz Salmón and Luis 2018, Lee *et al.* 2019, Peters and Hankins 2021). MD works at lower temperatures (50~70°C) than MSF or MED and thus can use low-grade waste heat and solar thermal energy sources (Choi *et al.* 2020, Peters and Hankins 2021, Usman *et al.* 2021). Moreover, MD runs at low hydrostatic

*Corresponding author, Professor,
E-mail: sanghlee@kookmin.ac.kr

pressures and thus membrane fouling in MD is expected to be less severe than in RO under similar conditions (Tijing *et al.* 2015, Janajreh *et al.* 2017). In addition, the theoretical rejection of non-volatile solutes such as inorganic ions by MD is 100% (Alkudhiri *et al.* 2012, Dantie and Choi 2017).

Four typical process configurations for MD are available, including the direct contact MD (DCMD), air gap MD (AGMD), vacuum MD (VMD), and sweeping gas MD (SGMD) (Tijing *et al.* 2015, González *et al.* 2017, Janajreh *et al.* 2017). In DCMD and AGMD, the difference between the feed temperature and the permeate (distillate) temperature in the membrane modules generates the chemical potential difference for the separation (Cerneau *et al.* 2009). On the other hand, in VMD and SGMD, the driving force is created by reducing the partial pressure of water vapor on the permeate side by using a vacuum or a sweeping gas, respectively (Cerneau *et al.* 2009). Although DCMD is the simplest configuration and has been preferentially used in laboratory-scale experiments, its practical application is hindered due to low thermal efficiency (Cerneau *et al.* 2009, Ashoor *et al.* 2016, Ullah *et al.* 2018). Instead, AGMD has been considered in pilot-scale research or commercial applications due to its higher performance ratio than DCMD (Leaper *et al.* 2019, Noor *et al.* 2020). However, AGMD has problems associated with low flux in comparison with DCMD or VMD (Alsaadi *et al.* 2015, Janajreh *et al.* 2017). The low flux in AGMD is attributed to the additional resistance created of water vapor transport by non-condensable gases in the air gap (Abu-Zeid *et al.* 2016, Janajreh *et al.* 2017).

One of the approaches to improving the flux and productivity of AGMD is the removal of non-condensable gases from the air gap by reducing the air gap pressure, which is done by a vacuum pump (Alsaadi *et al.* 2015, Abu-Zeid *et al.* 2016, Andrés-Mañas *et al.* 2020). This technique is called vacuum-assisted AGMD (V-AGMD) that can eliminate the drawbacks of the air gap and enhance the process performance (Andrés-Mañas *et al.* 2020, Kim *et al.* 2021). Unlike VMD, the water vapor condensates inside the module in V-AGMD. Therefore, no external condenser is required for V-AGMD (Alsaadi *et al.* 2015, Kim *et al.* 2021). The difference in the water productivity between AGMD and V-AGMD may be significant (Abu-Zeid *et al.* 2016). It has been reported that the flux in V-AGMD was 2 ~ 3 times higher than that in AGMD using the same membranes and feed temperature conditions (Gostoli *et al.* 1987, Guijt *et al.* 2005). Certainly, these results suggest that V-AGMD is a promising technique that enables high flux and high thermal efficiency. Nevertheless, relatively little information is available on V-AGMD due to insufficient data in the literature (Alsaadis *et al.* 2015, Abu-Zeid *et al.* 2016). Moreover, the possibility of membrane deformation, which has been reported in other membrane contactors (She *et al.* 2013, Barragán and Pastuschuk 2014, Blandin *et al.* 2016, Yuan *et al.* 2019, Lee *et al.* 2020), has not been considered in V-AGMD.

The goal of the present article is to investigate the performance of V-AGMD systems in various conditions. The effects of the feed temperature, vacuum pressure, air gap on the flux in V-AGMD were explored. Then, the

extent of the deformation for the MD membranes due to depressurization of the air gap was examined. Empirical and statistical models such as multilinear regression, general regression neural network (GNN), and multilayer feed-forward neural networks (MFNN) were developed to analyze the flux as a function of temperature difference, vacuum pressure, initial air gap depth, and the degree of membrane deformation. To the best knowledge of the authors, this is the first study reporting the deformation of membranes in the V-AGMD configuration, which may be an important issue to be addressed before the widespread application of the V-AGMD technique.

2. Materials and methods

2.1 Materials

The MD membranes (GVHP14250), which is made of hydrophobic polyvinylidene fluoride (PVDF), were purchased from Merck Millipore. According to the manufacturer, the membrane porosity is 75%, and the mean pore size and thickness of the membrane are 0.22 μm and 125 μm , respectively. Synthetic seawater (35,000 mg/L NaCl) was prepared and applied as the feed solution. The NaCl rejections were over 99.9% in all experiments, indicating that there was no pore wetting.

2.2 Membrane module

Fig. 1(a) shows the configuration of a laboratory-scale V-AGMD module. There are three major parts in the module, including the feed plate, the air gap plate, and the cooling water plate. The feed and cooling water plates were made of acrylic resin, while the air gap plate was made of stainless steel. The effective membrane area was 0.0012 m^2 . The depth, width, and length of the flow channels in the feed and cooling water channels were 2 mm, 20 mm, and 60 mm, respectively. The permeate outlet in the air gap plate was depressurized by applying vacuum, allowing the V-AGMD operation. To adjust the air gap depth, three air gap plates were fabricated, which have the air gap depth of 2 mm, 3 mm, and 4 mm, respectively. A spacer (34-mil reverse osmosis feed spacer, Hydranautics, U.S.A.) was inserted between the membrane and the air gap plate. The photograph of the V-AGMD module is shown in Fig. 1(b).

2.3 Experimental setup for V-AGMD

Fig. 2 shows the schematic diagram of the V-AGMD experimental equipment. Two gear pumps were used to recirculate the feed solution and the cooling water, respectively. The feed flow rate was 0.6 L/min and the cooling water flow rate was 0.4 L/min. Using a heater at the bottom of the feed tank, the temperature of the feed solution was regulated from 40°C to 80°C. Using a chiller connected to a water bath, the temperature of the cooling water was kept to 20°C. The water vapor passing through the MD membrane condensed on the surface of the air gap and then collected through the permeate outlet. The mass of the accumulated permeate was measured using an electronic balance, which sends data to a communication software on

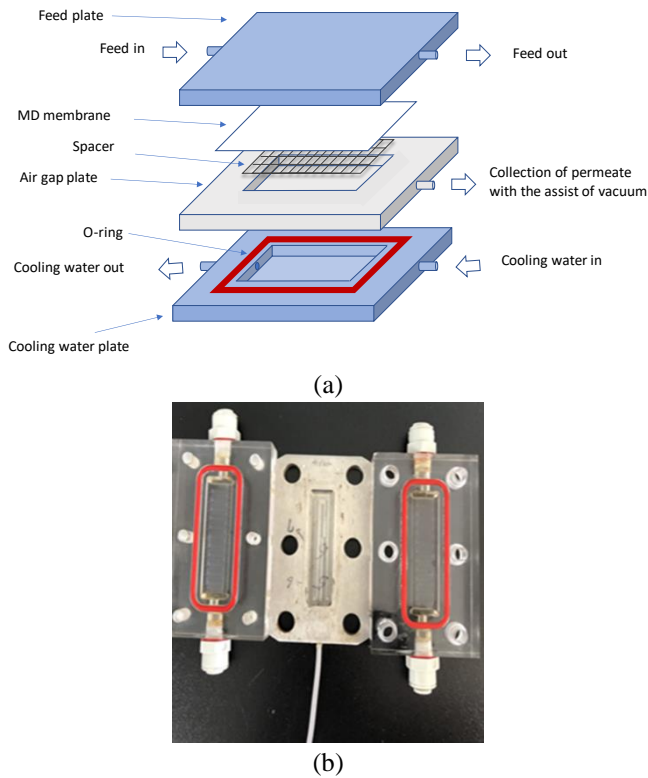


Fig. 1 (a) V-AGMD module configuration; (b) Photograph of V-AGMD module

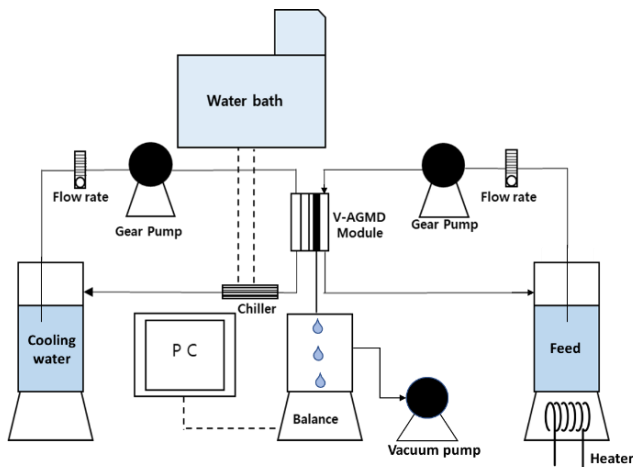


Fig. 2 Schematic diagram of laboratory-scale V-AGMD system

a computer. A vacuum pump was connected to the permeate line, which adjusted the vacuum pressure from -0.5 bar to -0.8 bar. Thus, the permeate pressure was in the range between 0.2 bar and 0.5 bar. It was not possible to maintain the vacuum pressure below -0.5 bar due to the limitation of the vacuum pump used in this paper. AGMD experiments were carried out without the use of the vacuum pump.

2.4 Experimental conditions and procedures

Table 1 presents the conditions of the experimental runs. Both AGMD and V-AGMD experiments were carried out to investigate the effect of vacuum pressure on the flux.

Table 1 Operating conditions for AGMD and V-AGMD experiments

No.	Temperature difference (ΔT)	Air gap width	Vacuum pressure	Flow rates
1	20°C	4 mm	0.0 bar	
2	30°C	4 mm	0.0 bar	
3	40°C	4 mm	0.0 bar	
4	50°C	4 mm	0.0 bar	
5	60°C	4 mm	0.0 bar	
6	20°C	4 mm	-0.8 bar	
7	30°C	4 mm	-0.8 bar	
8	40°C	4 mm	-0.8 bar	
9	50°C	4 mm	-0.8 bar	
10	60°C	4 mm	-0.8 bar	
11	40°C	3 mm	-0.5 bar	
12	40°C	3 mm	-0.6 bar	
13	40°C	3 mm	-0.7 bar	
14	40°C	3 mm	-0.8 bar	
15	30°C	4 mm	-0.5 bar	
16	40°C	4 mm	-0.5 bar	
17	50°C	4 mm	-0.5 bar	
18	30°C	4 mm	-0.6 bar	
19	40°C	4 mm	-0.6 bar	
20	50°C	4 mm	-0.6 bar	
21	30°C	4 mm	-0.7 bar	
22	40°C	4 mm	-0.7 bar	
23	50°C	4 mm	-0.7 bar	
24	40°C	2 mm	-0.5 bar	
25	40°C	2 mm	-0.6 bar	
26	40°C	2 mm	-0.7 bar	
27	40°C	2 mm	-0.8 bar	

Feed:
0.6 L/min
Permeate:
0.4 L/min

The temperature difference (ΔT), the air gap width, and vacuum pressures were varied to investigate their effect on flux values. The flow rates of the feed and permeate were maintained constant. Details on the experimental procedures for V-AGMD were reported elsewhere (Kim *et al.* 2021).

2.5 Scanning electron microscopy

After the V-AGMD experiments, the membrane samples were coated with Pt. Then the surfaces of the membranes were then examined by FE-SEM (FE-SEM 7800F Prime, JEOL Ltd. Japan) (Kim *et al.* 2021).

2.6 Measurement of liquid entry pressure

Liquid entry pressures (LEPs), the minimum pressure required for water to pass through the pores of the membrane, were also measured after the V-AGMD experiment. The LEP of the membranes was measured

using an in-house-developed LEP apparatus (Kim *et al.* 2021). DI water was placed in the water chamber and a membrane sample was placed on the device. Then, nitrogen gas was supplied to the water chamber. The pressure of nitrogen gas was increased until the first droplets were found on the membrane surface. At least three measurements were taken for each sample.

2.7 Model fit to experimental data

Two model fit approaches were attempted to analyze the experimental data: multiple linear regression (MLR) and artificial neural network (ANN). MLR is a statistical technique that uses several independent variables to fit the outcome of a dependent variable (Ebrahimzadeh *et al.* 2021). It aims at the development of the linear relationship between the independent variables and a dependent variable (Saadon *et al.* 2021). The following equation is used:

$$y = \beta_0 + \beta_1 x_1 + \beta_2 x_2 + \dots + \beta_n x_n + \varepsilon \quad (1)$$

where y is the dependent variable, x_1, x_2, \dots, x_i are the independent variables, $\beta_1, \beta_2, \dots, \beta_i$ are the regression coefficients, n is the number of independent variables, and ε is the model error. The MLR model is based on the following assumptions: There is a linear relationship between the independent variable and the dependent variable and the independent variables are not too highly correlated with each other. If these assumptions are not valid, the MLR model fails to fit the experimental data.

An artificial neural network (ANN) is an elaborated computation technique inspired by the architectures of biological neural networks (Bagher *et al.* 2019). It aims at the understanding of complex relationships between independent variables and the dependent variables (Bhagat *et al.* 2020). Two kinds of ANN techniques were considered in this work, including general regression neural networks (GNNs) and multilayer feedforward neural networks (MFNNs) (Roman *et al.* 2020). GNNs are one-pass learning algorithms that provide reasonable prediction capability even with sparse data (Niwa 2003). It has been shown that GNNs can be applied to any regression problem where an assumption of linearity is not justified (Niwa 2003). MFNNs, which are also called multilayer perceptrons (MLPs), fully connected networks with multiple single neurons. MFNNs consist of an input layer, hidden layers, and an output layer. MFNNs are designed to solve nonlinear problems. The major applications of MFNNs are pattern classification, recognition, prediction, and approximation.

To develop regression models, the data on V-AGMD experiments were collected and processed. The data points were derived from the time-series data of the flux, which was measured in every 1 min. The total number of the data points used for the modeling was 1212. The independent variables were the air gap depth, applied vacuum pressure, feed temperature, and the extent of deformation. Using these four variables, the flux was modeled using MLR, GNN, and MFNN algorithms. In the cases of ANN models, 80% of the data points were used for training and 20% were used for testing. The data for the model test were randomly selected. For MFNN models, the numbers of the nodes in

the 1st and 2nd layers were automatically determined. The MLR models were developed using the XLSTAT software (XLSTAT, Addinsoft, U.S.A.) and the GNN and MFNN models were developed using the NeuralTools software (Decision tools, Palisade, U.S.A.).

Based on the model fits, the relative variable impacts (RI) were estimated for the independent variables. The purpose of variable impact analysis is to measure the sensitivity of net predictions to changes in independent variables. As a result of the analysis, every independent variable is assigned a ‘‘Relative Variable Impact’’ value; these are percent values and add to 100%. The lower the percent value for a given variable, the less that variable affects the predictions.

The following method was applied to calculate the relative variable impact: To begin, the first case in the training set is taken, and the values of the first independent variable was varied while keeping other variables fixed. Predictions with our neural net were made and the values for the dependent variable were recoded. The difference between max and min dependent value is calculated as d . This procedure is repeated for every case in the training set. The mean Delta value for the i^{th} variable is denoted as $\bar{\delta}_i$. For $i = 1, 2, \dots, n$, $\bar{\delta}_1, \bar{\delta}_2, \dots, \bar{\delta}_n$ are calculated. Then the impact of the j^{th} variable (RI_j) is:

$$RI_j = \frac{\bar{\delta}_j}{\sum_i^n \bar{\delta}_i} \quad (2)$$

which is expressed as a percentage, and similarly for the others. The total impact is always 100%.

3. Results and discussion

3.1 Comparison of flux between AGMD and V-AGMD

To begin, a series of experiments were carried out to measure permeate flux as a function of time in the AGMD system (run no. 1~4). The temperature difference (ΔT) ranged from 20°C to 60°C, which corresponds to feed temperature in the range of 40°C and 80°C. The air gap width was 4 mm, and no vacuum was applied in these experiments to maintain the AGMD operation mode. The results are shown in Fig. 3. Since the feed water was a 35,000 mg/L NaCl solution, no flux decline was observed within 60 min, which indicates negligible potential of membrane wetting in the feed water. As expected, the flux increases as an increase in ΔT , which is attributed to an increase in the vapor pressure difference between the feed and the permeate. Nevertheless, the flux values were not high, ranging from 1.03 L/m²-hr ($\Delta T = 20^\circ\text{C}$) to 11.6 L/m²-hr ($\Delta T = 60^\circ\text{C}$). This result is in accordance with the previous reports on the low flux and productivity of AGMD systems (Yang *et al.* 2019).

Another set of experiments were performed with the application of vacuum (-0.8 bar) to the permeate line, which corresponds to the V-AGMD operation. All the other conditions were similar to those of the previous AGMD experiments. As shown in Fig. 4, significant improvements

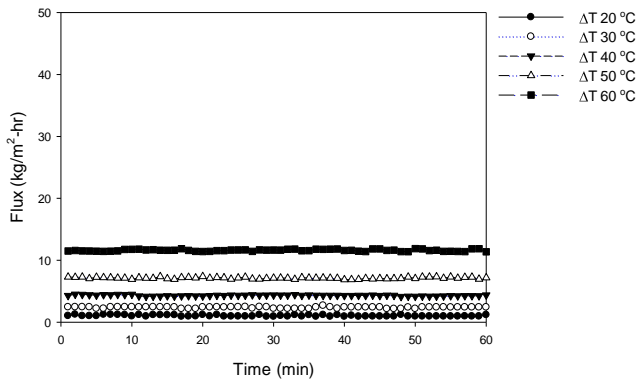


Fig. 3 Dependence of flux on temperature difference (ΔT) in AGMD system (Conditions: air gap width = 4 mm; vacuum pressure = 0 bar (no vacuum); feed flow rate = 0.6 L/min; permeate flow rate = 0.4 L/min)

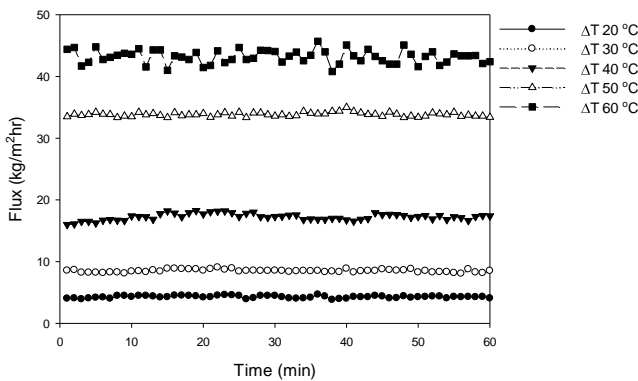


Fig. 4 Dependence of flux on temperature difference (ΔT) in V-AGMD system (Conditions: air gap width = 4 mm; vacuum pressure = -0.8 bar; feed flow rate = 0.6 L/min; permeate flow rate = 0.4 L/min)

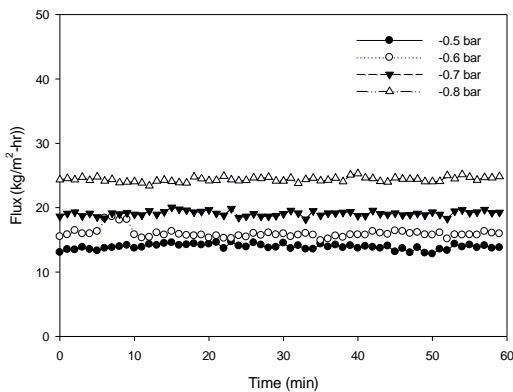


Fig. 5 Dependence of flux on vacuum pressure in V-AGMD system (Conditions: air gap width = 3 mm; vacuum pressure = 0 ~ -0.8 bar; temperature difference (ΔT) = 40; feed flow rate = 0.6 L/min; permeate flow rate = 0.4 L/min)

in flux were obtained in V-AGMD. The measured flux ranges from 4.3 L/m²-hr ($\Delta T = 20^\circ\text{C}$) to 43.2 L/m²-hr ($\Delta T = 60^\circ\text{C}$). This implies that the flux values in V-AGMD were 3.4 ~ 4.1 times higher than those in AGMD. The flux improvement in V-AGMD may be attributed to the removal

of non-condensable gas from the air gap by vacuum application (Alsaadi *et al.* 2015). The presence of the non-condensable gases reduces the water vapor transfer in the air gap. When they were removed from the air gap, which can be achieved under sub-atmospheric conditions, the rate of the water vapor transfer increase, leading to high flux. The flux was not reduced during the operating time in all cases. This indicates that there was no wetting issue in V-AGMD under the applied conditions. It appears that there is no change in the membrane properties that results in flux decline with time under V-AGMD operation.

3.2 Effect of vacuum pressure on flux in V-AGMD

To further investigate the effect of vacuum pressure on flux, V-AGMD operations were performed under the vacuum pressure ranging from -0.5 bar to -0.8 bar. The difference in temperature between the feed and the permeate (ΔT) was 40°C. It is evident from Fig. 5 that the flux becomes higher with a high degree of vacuum applied to the V-AGMD system. The flux was 13.9 L/m²-hr at the vacuum of -0.5 bar and increased up to 24.4 L/m²-hr at -0.8 bar. During the experiments, the flux and NaCl rejection were not changed, indicating that the properties of the membranes remained the same.

Fig. 6(a) shows the flux as a function of vacuum pressure and ΔT . The error bars indicate the standard deviations of the measured flux values. There are two significant trends in the results. First, the flux exponentially increases as the degree of vacuum increases. When the vacuum pressure changed from -0.5 bar to -0.6 bar, the flux increased by 14.7~17.9%. With the change in the vacuum pressure from -0.6 bar to -0.7 bar, the flux was improved by 23.5~25.3%. A further change in the vacuum from -0.7 bar to -0.8 bar increased the flux by 30.1~41.7%. Second, the V-AGMD operation at a higher ΔT resulted in a higher flux increase. When ΔT values were 30°C and 40°C, the flux values at -0.8 bar were 3.15 and 3.23 times higher than those at 0 bar, respectively. With ΔT of 50°C, the flux at -0.8 bar became 3.67 times higher than that at 0 bar. These results suggest that the application of V-AGMD is effective to increase flux under high vacuum degree and ΔT conditions.

In both AGMD and V-AGMD, the flux is affected by the air gap pressure. If the saturation pressure of water vapor is higher than the air gap pressure, the water vapor transfer rate becomes higher. Fig. 6(b) shows the flux as a function of the difference between the air gap pressure and the saturation pressure of water vapor. According to the steam table, the saturation pressures at 50°C, 60°C, and 70°C are 0.1235 bar, 0.1994 bar, and 0.3119 bar, respectively (El-Dessouky and Ettouney 2002). Since the air gap pressure in AGMD is 1 bar, the pressure differences at 50°C, 60°C, and 70°C are 0.876 bar, 0.801 bar, and 0.688 bar, respectively. A linear relationship between the flux in AGMD and the pressure difference was obtained (black symbols in the plot) with the R^2 value of 0.999, indicating the enhanced mass transfer of water vapor at low air gap pressures. Similar trends were observed in the case of V-AGMD (white symbols in the plot).

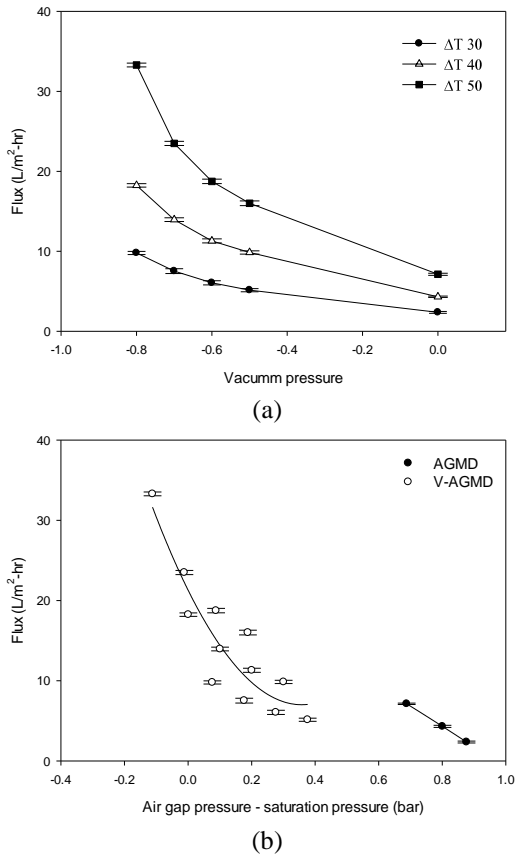


Fig. 6 (a) Effect of vacuum pressure and temperature difference (ΔT) on flux in AGMD and V-AGMD systems (b) Correlations between the difference between air gap pressure and saturation pressure and flux in AGMD and V-AGMD (Conditions: air gap width = 4 mm; vacuum pressure = 0 ~ -0.8 bar; temperature difference (ΔT) = 30 ~ 50°C; feed flow rate = 0.6 L/min; permeate flow rate = 0.4 L/min)

However, the relationship between the flux in AGMD and the pressure difference does not seem to be linear because the R^2 for a linear regression was less than 0.749. It should be noted that the dependence of the V-AGMD flux on the pressure difference is different from that of the AGMD. This suggests that the mass transfer mechanisms in V-AGMD are different from that in AGMD. If non-condensable gases have high partial pressure in the air gap, which corresponds to conventional AGMD, the mass transfer is dominated by the molecular diffusion mechanism (Im *et al.* 2018). On the other hand, the diffusive mass transfer mechanism becomes insignificant as the non-condensable gases are removed in the case of V-AGMD (Alsaadi *et al.* 2015). Nevertheless, the difference of the flux trend (linear or non-linear trend) with respect to pressure difference cannot be solely caused by the difference of the mass transfer mechanism because the range of the pressure difference for AGMD and V-AGMD are different. A more quantitative analysis will be necessary to separate the effect of the mass transfer mechanisms from the other effects in the future. Currently, it can be concluded that the difference in the mass transfer mechanisms between

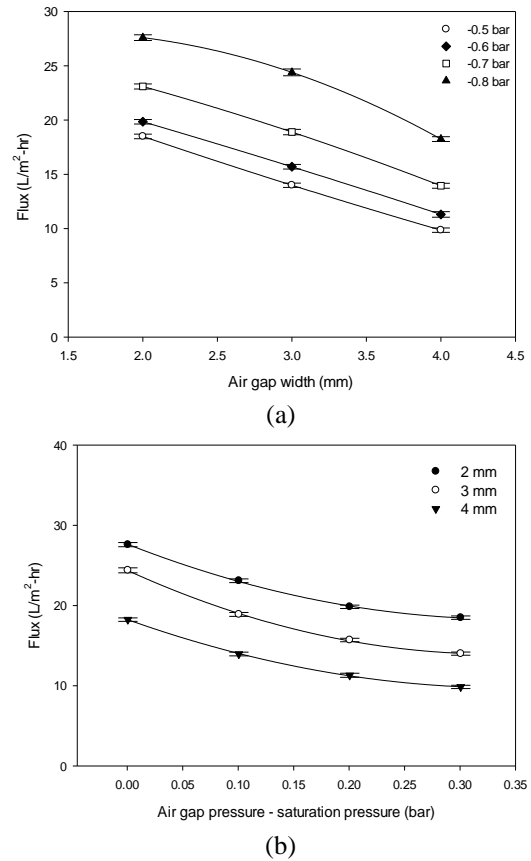


Fig. 7 Effect of air gap width and vacuum pressure on flux in V-AGMD system (Conditions: air gap width = 2 ~ 4 mm; vacuum pressure = -0.5 ~ -0.8 bar; temperature difference (ΔT) = 40°C; feed flow rate = 0.6 L/min; permeate flow rate = 0.4 L/min)

AGMD and V-AGMD is one of the factors affecting the flux patterns.

3.3 Effect of air gap width on flux in V-AGMD

The variations in flux in V-AGMD under different vacuum pressures and air gap widths are shown in Fig. 7(a). With an increase in the degree of vacuum, the flux increases in all cases, which matches the results in Fig. 6(a). When the air gap width decrease, the flux increases due to the reduction in mass transfer resistance of the air gap. The flux becomes 1.51~1.88 times higher as the air gap width is reduced from 4 mm to 2 mm. As can be seen in Fig. 7(b), the flux could be correlated with the difference between the air gap pressure and the saturation pressure of water vapor. An increase in the pressure difference results in a decrease in the flux. This can be also attributed to the enhanced mass transfer of water vapor under low air gap pressure conditions.

3.4 Deformation of the membrane due to vacuum pressure

The previous results demonstrate the positive effect of the vacuum for increasing the flux in V-AGMD. However, it was found that there may be a negative effect of the

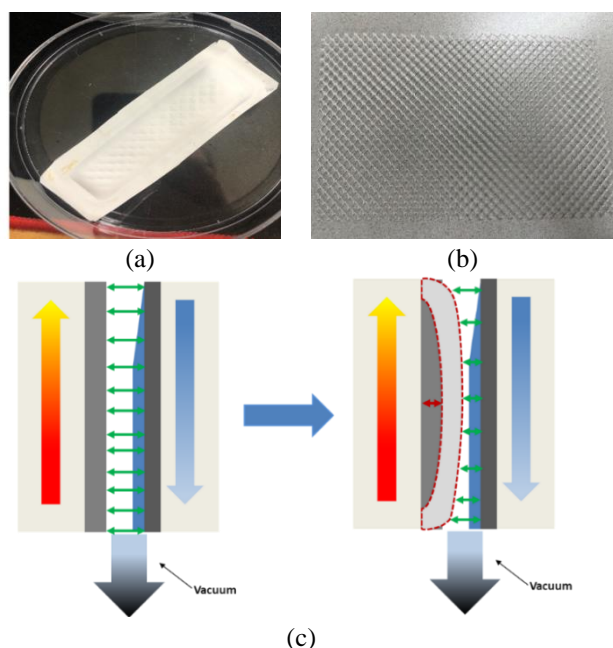


Fig. 8 Deformation of MD membranes due to applied vacuum (a) An example of deformed membrane after the V-AGMD experiment (b) photograph of the spacer (c) Mechanism of membrane deformation

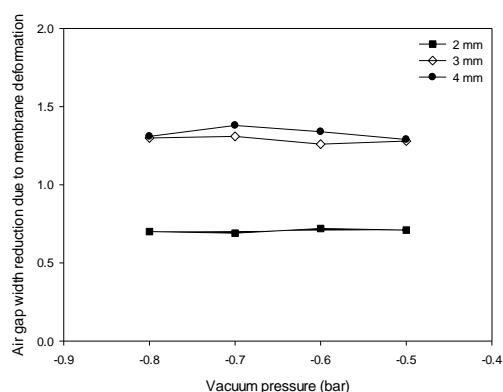


Fig. 9 Effect of vacuum pressure on reduction in air gap width (Conditions: vacuum pressure = -0.5 ~ -0.8 bar; temperature difference (ΔT) = 40°C; feed flow rate = 0.6 L/min; permeate flow rate = 0.4 L/min)

vacuum due to the deformation of the membranes. Fig. 8(a) presents the image of the membranes after the V-AGMD operation. It is evident that the membrane was deformed due to the application of negative pressure in V-AGMD. Although the net-type spacer (Fig. 8(b)) was used to support the membrane, the membrane deformation occurred. The spacer created patterns on the membrane surface as shown in Fig. 8(a).

The membrane deformation is further schematically illustrated in Fig. 8(c). If the membrane is operated in V-AGMD, it is unsupported and may be deformed due to the applied vacuum on the air gap side. Although the spacer is used to support the membrane, it is not enough to prevent the deformation. Moreover, the membrane area between the spacer filaments cannot be fully supported. Although the

Table 2 Operating conditions for AGMD and V-AGMD experiments

Membrane	Conditions	NaCl rejection	Liquid entry pressure (bar)
Intact membrane (AGMD)	Feed temperature: 60°C Air gap width: 4 mm	> 99.9 %	1.91 ± 0.22 bar
Deformed membrane with spacer (V-AGMD)	Feed temperature: 60°C Air gap width: 4 mm Vacuum: -0.8 bar	> 99.9 %	1.91 ± 0.22 bar
Deformed membrane without spacer (V-AGMD)	Feed temperature: 60°C Air gap width: 4 mm Vacuum: -0.8 bar	< 50 %	< 0.5 bar

results are not included, V-AGMD experiments were carried out without the use of the spacer, resulting in damage to the membranes. This suggests that the use of spacer mitigates the deformation but cannot prevent it.

As illustrated in Fig. 8(c), the membrane deformation results in a reduction in the air gap width. As the membrane becomes concave, the effective distance between the membrane support and the air gap wall decreases. To quantify this, the reduction in the air gap due to the deformation was measured using a vernier caliper. Fig. 9 shows the air gap reduction as a function of the vacuum pressure and the initial air gap width. When the air gap width was 2 mm, the air gap reduction was relatively small, ranging from 0.69 mm to 0.72 mm. With the larger air gap widths, the air gap reduction was larger, which is in the range of 1.26 mm to 1.38 mm. It is evident that the vacuum pressure significantly affects the air gap reduction. Nevertheless, as long as the vacuum pressure exceeds -0.5 bar, the extents of air gap reduction were similar. This may be attributed to the fact that the spacer partially supports the membrane to prevent extreme deformation.

To evaluate the effect of the deformation on the separation properties of the membranes, the NaCl rejection and LEP were measured for the deformed membranes. As shown in Table 2, there was no difference in NaCl rejection between AGMD and V-AGMD with the spacer (> 99.9%). In addition, the LEP values were the same (1.91 bar). This suggests that the separation capability of the membranes is not changed by the deformation at least within the operation time in the study (1 hour). On the other hand, the rejection and LEP became low in V-AGMD operation without the use of the spacer, as can be seen in Table 2. Obviously, the membranes without the spacer were damaged by the pressure difference.

After the V-AGMD operation, the membranes were examined using the SEM technique. Fig. 10(a) shows the SEM image of the intact membrane and Figs. 10(b)-10(d) present the SEM images after V-AGMD operations with different air gap widths. Compared with Fig. 10(a), the SEM image in Fig. 10(b), which corresponds to V-AGMD operation with the air gap width of 4 mm at -0.5 bar, is not different. This indicates that the microstructure of the membrane is the same at low vacuum pressure (-0.5 bar) even with the occurrence of the deformation. A similar

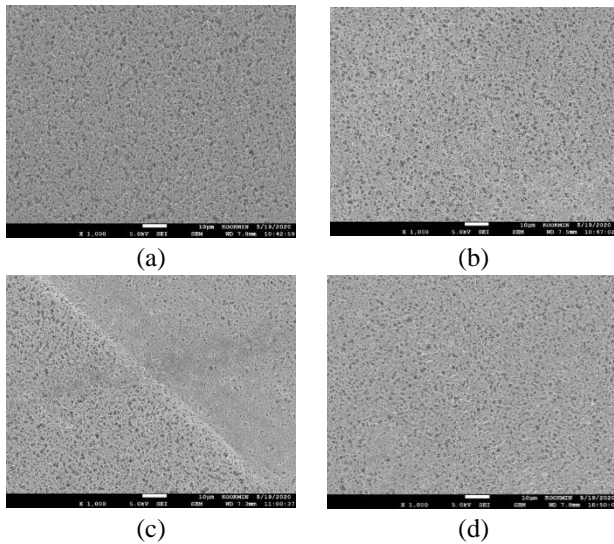


Fig. 10 SEM images of membranes before and after V-AGMD experiments. (a) intact membrane (b) used membrane (air gap width = 4 mm, vacuum pressure = -0.5 bar) (c) used membrane (air gap width = 4 mm, vacuum pressure = -0.8 bar) (d) used membrane (air gap width = 2 mm, vacuum pressure = -0.8 bar)

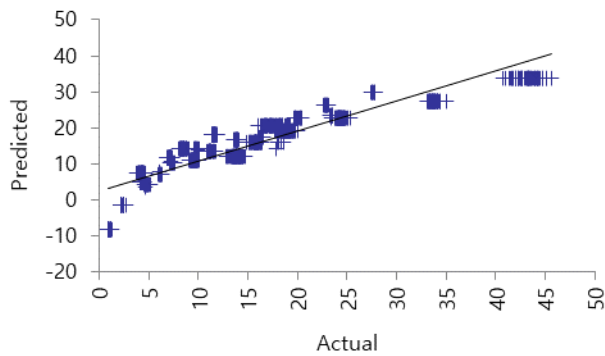


Fig. 11 Multi-linear regression model fit (a) Comparison of experimental results and model fit (b) Relative variable impacts

result was observed in Fig. 10(d), which corresponds to V-AGMD operation with the air gap width of 2 mm at -0.8 bar. Since the air gap width was small (2 mm), the changes in the microstructure of the membrane seem to be negligible. On the contrary, the membrane structure was clearly different in Fig. 10(c), corresponding to V-AGMD operation with the air gap width of 4 mm at -0.8 bar. Due to the large air gap width and high vacuum pressure, the degree of the membrane deformation appears to be high. The membrane area that contacted the filament of the spacer was pressurized, leading to a reduction in the pore size. But the other area of the membrane does not seem to be changed. The salt rejection of MD membranes is affected by pore wetting, which is related to the maximum pore size. The LEP is also dependent on the maximum pore size. Since the pore sizes of the membranes after V-AGMD operation did not increase, the salt rejection and LEP should be the same. Accordingly, the results in Table 2 are supported by the findings from the SEM analysis.

Although the membrane deformation did not change the rejection and LEP of the membranes during short-term experiments of V-AGMD process with the spacer, its long-term effect on membrane properties needs to be assessed to ensure the feasibility of V-AGMD for practical applications. The effect of the spacer shape and dimensions on the membrane deformation needs to be investigated. The scope of this work is to report the impact of membrane deformation and thus will provide insight into further development of V-AGMD modules and processes.

3.5 Model fit to flux in V-AGMD with membrane deformation

Since many factors are affecting the performance of the V-AGMD process, it is difficult to interpret the flux using theoretical models. There have been several works on mathematical modeling of AGMD and V-AGMD processes (Alkudhiri *et al.* 2012, Alsaadi *et al.* 2015, Janajreh *et al.* 2017, Im *et al.* 2018), the effect of the membrane deformation on flux has not been considered yet. When the deformation occurs, the effective air gap width decreases (Fig. 8(c)), thereby increasing the flux due to a reduction in the mass transfer resistance. To quantify this effect, complex modeling approaches based on computation fluid dynamics (CFD) are required due to irregular patterns of the membrane deformation. Moreover, the flux is influenced by the feed temperature and the vacuum pressure. Accordingly, a simple mathematical model cannot be used to analyze the V-AGMD flux.

In this study, several statistical modeling techniques were attempted as alternative approaches. First, a regression model was developed based on the MLR technique. The response (dependent variable) is the flux and the independent variables are the air gap width, the vacuum pressure, the feed temperature, and the degree of the membrane deformation. As shown in Fig. 11, the MLR model can match the experimental data to a certain degree. Nevertheless, the model fit was not successful when the flux is either below 5 L/m²-hr or above 28 L/m²-hr. The R² value is 0.827, indicating that the MLR model is not sufficient to interpret the V-AGMD flux. This can be attributed to the limited capability of MLR models for the analysis of nonlinear phenomena such as V-AGMD operation.

To achieve a better fit, a GNN model was developed instead of the MLR model. As a neural network model, the development of GNN model includes the training and testing steps. Fig. 12(a) shows the results on the training of the GNN model using 80% of the experimental data. Compared with the MLR model, the GNN model matches the experimental results well, resulting in the R² of 0.9983. The results on the GNN model test using 20% of the experimental data are also similar to those on the GNN model training, which is illustrated in Fig. 12(b). The R² is also 0.9983 in the case of the GNN model test. This is because GNN uses a neural network algorithm to interpret nonlinear phenomena. Based on these results, the relative impacts of the independent variables were calculated, as shown in Fig. 12(c). The temperature is found to have the

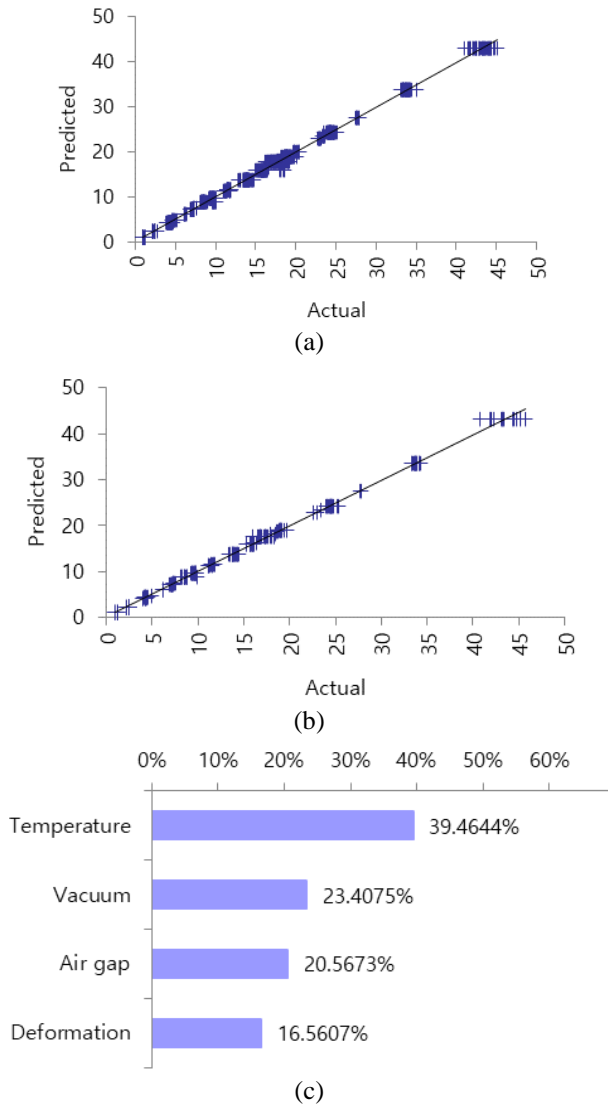


Fig. 12 General regression neural network (GNN) model fit (a) Training results (b) Test results (c) Relative variable impacts

highest impact (39.4%). The impacts of the air gap width and the vacuum pressure are similar (approximately 20.56%). The degree of the deformation has also an impact of 16.56%, suggesting that its impact is not negligible.

In addition to the GNN model, a MLFNN model was also considered and developed as an alternative method. Based on the search for the best network structures, the nodes of the 1st and the 2nd layers were determined to be 3 and 2, respectively. The training and test results of the MLFNN model are shown in Figs. 13(a) and 13(b), respectively. The corresponding R^2 values are 0.9976 and 0.9971, suggesting that the model successfully matches the experimental results. Although the R^2 values of the GNN and MLFNN models are not the same, the difference is negligible and statistically insignificant. Fig. 13(c) shows the relative impacts of the independent variables. Similar to the case of the GNN model, the temperature is estimated to have the highest impact. The relative impact of the deformation is 4.48%, which is significantly lower than that

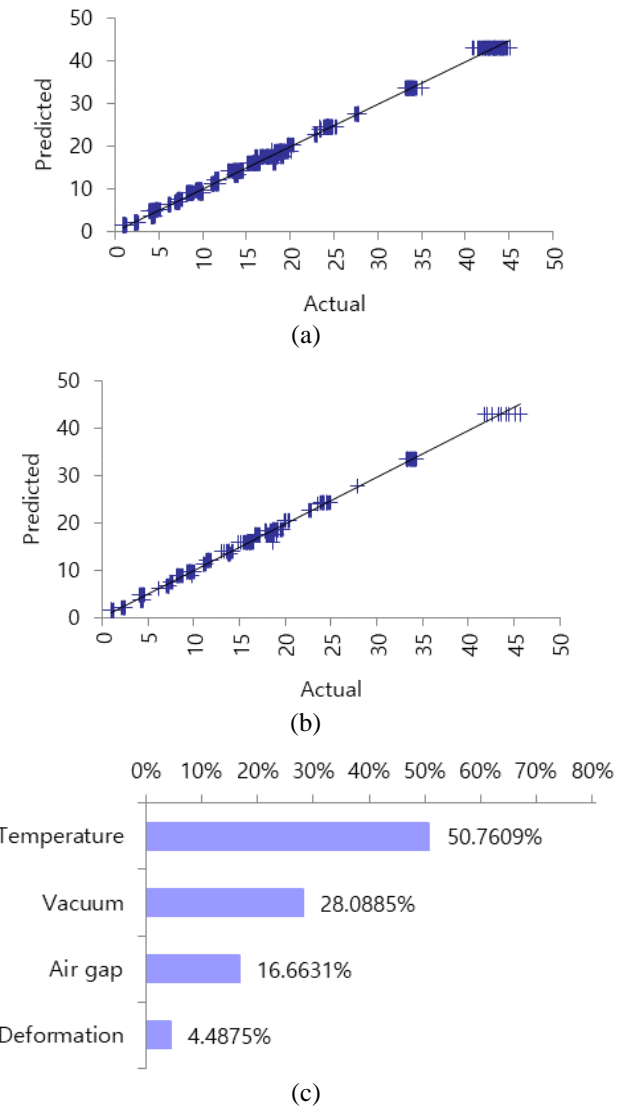


Fig. 13 Multilayer feedforward neural networks (MLFNN) model fit (a) Training results (b) Test results (c) Relative variable impacts

of the GNN model. The relative impacts are calculated using Eq. (2). It is interesting to note that GNN and MLFNN models exhibit different values of the relative variable impacts. Since both GNN and MLFNN are “black-box” models, it is not possible to explain the reason in terms of the model structure. Nevertheless, the rank of the relative variable impacts is the same (temperature > vacuum > air gap > deformation). In summary, both GNN and MLFNN models can reasonably fit the experimental data and the estimated relative impact of the membrane deformation ranges from 4.48% to 16.56%.

4. Conclusions

In this study, the effect of vacuum pressure on flux and membrane deformation in V-AGMD was investigated. The following conclusions were withdrawn from the results:

1. The application of vacuum, ranging from -0.5 bar to

-0.8 bar, on the air gap resulted in significant flux improvements. The V-AGMD flux was 3.4 ~ 4.1 times higher than the AGMD flux under the same feed temperature and air gap width.

2. The flux in both AGMD and V-AGMD is inversely proportional to the difference between the air gap pressure and the saturation pressure of water vapor. This is attributed to the enhancement of the mass transfer in the air gap. Nevertheless, the dependence of the V-AGMD flux on the pressure difference is different from that of the AGMD, suggesting that the mass transfer mechanisms in V-AGMD are different from that in AGMD.

3. After the V-AGMD operation, the membranes were found to be deformed due to the pressure difference between the feed and the air gap sides. The flat-sheet membranes were not fully supported by the spacer, they were deformed due to the applied vacuum on the air gap side. The deformation resulted in a reduction in the effective air gap width. The rejection and LEP were not changed after the V-AGMD experiments, suggesting that the separation capability of the membranes was not compromised. Nevertheless, the long-term effect of vacuum pressure on membrane properties may be examined in the future.

4. The flux behaviors in V-AGMD were not successfully interpreted by the MLR model due to their nonlinear characteristics. On the other hand, neural network models, such as GNN and MLFNN, were able to fit the V-AGMD flux. According to the model calculations, the relative impacts of the membrane deformation were in the range between 4.48% to 16.56%.

Acknowledgment

This study was supported by the National Research of Korea (NRF-2021R1A2C1013611).

References

- Abu-Zeid, M.A.E.R., Zhang, L., Jin, W.Y., Feng, T., Wu, Y. and Chen, H. L. (2016), "Improving the performance of the air gap membrane distillation process by using a supplementary vacuum pump", *Desalination*, **384**, 31-42. <https://doi.org/10.1016/j.desal.2016.01.020>.
- Ahmed, F.E., Hashaikeh, R. and Hilal, N. (2020), "Hybrid technologies, The future of energy efficient desalination – A review", *Desalination*, **495**, 114659. <https://doi.org/10.1016/j.desal.2020.114659>.
- Ali, A., Tufa, R.A., Macedonio, F., Curcio, E. and Drioli, E. (2018), "Membrane technology in renewable-energy-driven desalination", *Renew. Sust. Energ. Rev.*, **81**, 1-21. <https://doi.org/10.1016/j.rser.2017.07.047>.
- Alkudhiri, A., Darwish, N. and Hilal, N. (2012), "Membrane distillation, A comprehensive review", *Desalination*, **287**, 2-18. <https://doi.org/10.1016/j.desal.2011.08.027>.
- Alsaadi, A.S., Francis, L., Maab, H., Amy, G.L. and Ghaffour, N. (2015), "Evaluation of air gap membrane distillation process running under sub-atmospheric conditions: Experimental and simulation studies", *J. Membr. Sci.*, **489**, 73-80. <https://doi.org/10.1016/j.memsci.2015.04.008>.
- Alsebaei, M.K. and Ahmad, A.L. (2020), "Membrane distillation, Progress in the improvement of dedicated membranes for enhanced hydrophobicity and desalination performance", *J. Ind. Eng. Chem.*, **86**, 13-34. <https://doi.org/10.1016/j.jiec.2020.03.006>.
- Altaee, A., Zaragoza, G. and van Toningen, H.R. (2014), "Comparison between forward osmosis-reverse osmosis and reverse osmosis processes for seawater desalination", *Desalination*, **336**(1), 50-57. <https://doi.org/10.1016/j.desal.2014.01.002>.
- Andrés-Mañas, J.A., Ruiz-Aguirre, A., Acién, F.G. and Zaragoza, G. (2020), "Performance increase of membrane distillation pilot scale modules operating in vacuum-enhanced air-gap configuration", *Desalination*, **475**, 114202. <https://doi.org/10.1016/j.desal.2019.114202>.
- Ashoor, B.B., Mansour, S., Giwa, A., Dufour, V. and Hasan, S.W. (2016), "Principles and applications of direct contact membrane distillation (DCMD): A comprehensive review", *Desalination*, **398**, 222-246. <https://doi.org/10.1016/j.desal.2016.07.043>.
- Atab, M.S., Smallbone, A.J. and Roskilly, A.P. (2016), "An operational and economic study of a reverse osmosis desalination system for potable water and land irrigation", *Desalination*, **397**, 174-184. <https://doi.org/10.1016/j.desal.2016.06.020>.
- Aziz, N.I.H.A. and Hanafiah, M.M. (2021), "Application of life cycle assessment for desalination: Progress, challenges and future directions", *Environ. Pollut.*, **268**, 115948. <https://doi.org/10.1016/j.envpol.2020.115948>.
- Bagheri, M., Akbari, A. and Mirbagheri, S.A. (2019), "Advanced control of membrane fouling in filtration systems using artificial intelligence and machine learning techniques, A critical review", *Proc. Safe. Environ. Protect.*, **123**, 229-252. <https://doi.org/10.1016/j.psep.2019.01.013>.
- Barragán, V.M. and Pastuschuk, E. (2014), "Viscoelastic deformation of sulfonated polymeric cation-exchange membranes exposed to a pressure gradient", *Mater. Chem. Phys.*, **146**(1), 65-72. <https://doi.org/10.1016/j.matchemphys.2014.02.043>.
- Bhagat, S.K., Tung, T.M. and Yaseen, Z.M. (2020), "Development of artificial intelligence for modeling wastewater heavy metal removal: State of the art, application assessment and possible future research", *J. Clean. Prod.*, **250**, 119473. <https://doi.org/10.1016/j.jclepro.2019.119473>.
- Blandin, G., Vervoort, H., D'Haese, A., Schoutteten, K., Bussche, J.V., Vanhaecke, L., Myat, D.T., Le-Clech, P. and Verliefe, A.R.D. (2016), "Impact of hydraulic pressure on membrane deformation and trace organic contaminants rejection in pressure assisted osmosis (PAO)", *Proc. Safe. Environ. Protect.*, **102**, 316-327. <https://doi.org/10.1016/j.psep.2016.04.004>.
- Caldera, U. and Breyer, C. (2020), "Strengthening the global water supply through a decarbonised global desalination sector and improved irrigation systems", *Energy*, **200**, 117507. <https://doi.org/10.1016/j.energy.2020.117507>.
- Cerneaux, S., Strużyńska, I., Kujawski, W.M., Persin, M. and Larbot, A. (2009), "Comparison of various membrane distillation methods for desalination using hydrophobic ceramic membranes", *J. Membr. Sci.*, **337**(1), 55-60. <https://doi.org/10.1016/j.memsci.2009.03.025>.
- Choi, Y., Lee, Y., Shin, K., Park, Y. and Lee, S. (2020), "Analysis of long-term performance of full-scale reverse osmosis desalination plant using artificial neural network and tree model", *Environ. Eng. Res.*, **25**(5), 763-770. <https://doi.org/10.4491/eer.2019.324>.
- Damtie, M.M. and Choi, J.S. (2017), "Modeling and application of direct contact membrane distillation for fluoride removal from aqueous solutions", *Desalin. Water Treat.*, **97**, 23-40. <https://doi.org/10.5004/dwt.2017.21690>.
- Dolan, F., Lamontagne, J., Link, R., Hejazi, M., Reed, P. and

- Edmonds, J. (2021), "Evaluating the economic impact of water scarcity in a changing world", *Nature Commun.*, **12**(1), 1915. <https://doi.org/10.1038/s41467-021-22194-0>.
- Drioli, E., Ali, A. and Macedonio, F. (2015), "Membrane distillation, Recent developments and perspectives", *Desalination*, **356**, 56-84. <https://doi.org/10.1016/j.desal.2014.10.028>.
- Ebrahimzadeh, S., Wols, B., Azzellino, A., Martijn, B.J. and van der Hoek, J.P. (2021), "Quantification and modelling of organic micropollutant removal by reverse osmosis (RO) drinking water treatment", *J. Water Proc. Eng.*, **42**, 102164. <https://doi.org/10.1016/j.jwpe.2021.102164>.
- El-Dessouky, H.T. and Ettouney, H.M. (2002), *Fundamentals of seawater desalination*, Elsevier.
- Goh, P.S., Lau, W.J., Othman, M.H.D. and Ismail, A.F. (2018), "Membrane fouling in desalination and its mitigation strategies", *Desalination*, **425**, 130-155. <https://doi.org/10.1016/j.desal.2017.10.018>.
- González, D., Amigo, J. and Suárez, F. (2017), "Membrane distillation, Perspectives for sustainable and improved desalination", *Renew. Sust. Energ. Rev.*, **80**, 238-259. <https://doi.org/10.1016/j.rser.2017.05.078>.
- Gostoli, C., Sarti, G.C. and Matulli, S. (1987), "Low temperature distillation through hydrophobic membranes", *Sep. Sci. Technol.*, **22**(2-3), 855-872. <https://doi.org/10.1080/01496398708068986>.
- Guijt, C.M., Meindersma, G.W., Reith, T. and De Haan, A.B. (2005), "Air gap membrane distillation: 2. Model validation and hollow fibre module performance analysis", *Sep. Purif. Technol.*, **43**(3), 245-255. <https://doi.org/10.1016/j.seppur.2004.09.016>.
- Hamdan, H., Saïdy, M., Alameddine, I. and Al-Hindi, M. (2021), "The feasibility of solar-powered small-scale brackish water desalination units in a coastal aquifer prone to saltwater intrusion: A comparison between electro dialysis reversal and reverse osmosis", *J. Environ. Manage.*, **290**, 112604. <https://doi.org/10.1016/j.jenvman.2021.112604>.
- Ihsanullah, I., Atieh, M.A., Sajid, M. and Nazal, M.K. (2021), "Desalination and environment: A critical analysis of impacts, mitigation strategies, and greener desalination technologies", *Sci. Total Environ.*, **780**, 146585. <https://doi.org/10.1016/j.scitotenv.2021.146585>.
- Im, B.G., Lee, J.G., Kim, Y.D. and Kim, W.S. (2018), "Theoretical modeling and simulation of AGMD and LGMD desalination processes using a composite membrane", *J. Membr. Sci.*, **565**, 14-24. <https://doi.org/10.1016/j.memsci.2018.08.006>.
- Janajreh, I., El Kadi, K., Hashaikeh, R. and Ahmed, R. (2017), "Numerical investigation of air gap membrane distillation (AGMD), Seeking optimal performance", *Desalination*, **424**, 122-130. <https://doi.org/10.1016/j.desal.2017.10.001>.
- Janajreh, I., Hashaikeh, R. and Hussain, M.N. (2017), "Evaluation of thermal efficiency of membrane distillation under conductive layer integration", *Energy Procedia*, **105**, 4935-4942. <https://doi.org/10.1016/j.egypro.2017.03.985>.
- Jiang, X., Shao, Y., Sheng, L., Li, P. and He, G. (2021), "Membrane crystallization for process intensification and control: A review", *Engineering*, **7**(1), 50-62. <https://doi.org/10.1016/j.eng.2020.06.024>.
- Kim, J., Park, K., Yang, D.R. and Hong, S. (2019), "A comprehensive review of energy consumption of seawater reverse osmosis desalination plants", *Appl. Energ.*, **254**, 113652. <https://doi.org/10.1016/j.apenergy.2019.113652>.
- Kim, Y., Choi, Y., Choi, J. and Lee, S. (2021), "Powdered activated carbon (PAC) – vacuum-assisted air gap membrane distillation (V-AGMD) hybrid system to treat wastewater containing surfactants, Effect of operating conditions", *Environ. Eng. Res.*, **26**(5), 200377-200370. <https://doi.org/10.4491/eer.2020.377>.
- Kundzewicz, Z.W., Krysanova, V., Benestad, R.E., Hov, Ø., Piniewski, M. and Otto, I.M. (2018), "Uncertainty in climate change impacts on water resources", *Environ. Sci. Policy*, **79**, 1-8. <https://doi.org/10.1016/j.envsci.2017.10.008>.
- Leaper, S., Abdel-Karim, A., Gad-Allah, T.A. and Gorgojo, P. (2019), "Air-gap membrane distillation as a one-step process for textile wastewater treatment", *Chem. Eng. J.*, **360**, 1330-1340. <https://doi.org/10.1016/j.cej.2018.10.209>.
- Lee, S., Choi, J., Park, Y.G., Shon, H., Ahn, C.H. and Kim, S.H. (2019), "Hybrid desalination processes for beneficial use of reverse osmosis brine: Current status and future prospects", *Desalination*, **454**, 104-111. <https://doi.org/10.1016/j.desal.2018.02.002>.
- Lee, C., Jang, J., Tin, N.T., Kim, S., Tang, C.Y. and Kim, I.S. (2020), "Effect of spacer configuration on the characteristics of FO membranes: Alteration of permeation characteristics by membrane deformation and concentration polarization", *Environ. Sci. Technol.*, **54**(10), 6385-6395. <https://doi.org/10.1021/acs.est.9b06921>.
- Missimer, T.M. and Maliva, R.G. (2018), "Environmental issues in seawater reverse osmosis desalination: Intakes and outfalls", *Desalination*, **434**, 198-215. <https://doi.org/10.1016/j.desal.2017.07.012>.
- Niwa, T. (2003), "Using general regression and probabilistic neural networks to predict human intestinal absorption with topological descriptors derived from two-dimensional chemical structures", *J. Chem. Inform. Comput. Sci.*, **43**(1), 113-119. <https://doi.org/10.1021/ci020013r>.
- Noor, I.E., Martin, A. and Dahl, O. (2020), "Process design of industrial-scale membrane distillation system for wastewater treatment in nano-electronics fabrication facilities", *MethodsX*, **7**, 101066. <https://doi.org/10.1016/j.mex.2020.101066>.
- Peters, C.D. and Hankins, N.P. (2021), "Making zero-liquid discharge desalination greener: Utilising low-grade heat and vacuum membrane distillation for the regeneration of volatile draw solutes", *Desalination*, **507**, 115034. <https://doi.org/10.1016/j.desal.2021.115034>.
- Pinto, F.S. and Marques, R.C. (2017), "Desalination projects economic feasibility: A standardization of cost determinants", *Renew. Sust. Energ. Rev.*, **78**, 904-915. <https://doi.org/10.1016/j.rser.2017.05.024>.
- Pistocchi, A., Bleninger, T., Breyer, C., Caldera, U., Dorati, C., Ganora, D., Millán, M.M., Paton, C., Poullis, D., Herrero, F.S., Sapiano, M., Semiat, R., Sommariva, C., Yucee, S. and Zaragoza, G. (2020), "Can seawater desalination be a win-win fix to our water cycle?", *Water Res.*, **182**, 115906. <https://doi.org/10.1016/j.watres.2020.115906>.
- Qasim, M., Badrelzaman, M., Darwish, N.N., Darwish, N.A. and Hilal, N. (2019), "Reverse osmosis desalination, A state-of-the-art review", *Desalination*, **459**, 59-104. <https://doi.org/10.1016/j.desal.2019.02.008>.
- Roman, N.D., Bre, F., Fachinotti, V.D. and Lamberts, R. (2020), "Application and characterization of metamodels based on artificial neural networks for building performance simulation, A systematic review", *Energ. Buildings*, **217**, 109972. <https://doi.org/10.1016/j.enbuild.2020.109972>.
- Ruiz Salmón, I. and Luis, P. (2018), "Membrane crystallization via membrane distillation", *Chem. Eng. Process*, **123**, 258-271. <https://doi.org/10.1016/j.cep.2017.11.017>.
- Saadon, A., Abdullah, J., Muhammad, N.S., Ariffin, J. and Julien, P.Y. (2021), "Predictive models for the estimation of riverbank erosion rates", *Catena*, **196**, 104917. <https://doi.org/10.1016/j.catena.2020.104917>.
- She, Q., Hou, D., Liu, J., Tan, K.H. and Tang, C.Y. (2013), "Effect of feed spacer induced membrane deformation on the performance of pressure retarded osmosis (PRO): Implications

- for PRO process operation”, *J. Membr. Sci.*, **445**, 170-182.
<https://doi.org/10.1016/j.memsci.2013.05.061>.
- Skuse, C., Gallego-Schmid, A., Azapagic, A. and Gorgojo, P. (2021), “Can emerging membrane-based desalination technologies replace reverse osmosis?”, *Desalination*, **500**, 114844. <https://doi.org/10.1016/j.desal.2020.114844>.
- Thomas, N., Mavukkandy, M.O., Loutatidou, S. and Arafat, H.A. (2017), “Membrane distillation research & implementation, Lessons from the past five decades”, *Sep. Purif. Technol.*, **189**, 108-127. <https://doi.org/10.1016/j.seppur.2017.07.069>.
- Tijing, L.D., Woo, Y.C., Choi, J.S., Lee, S., Kim, S.H. and Shon, H.K. (2015), “Fouling and its control in membrane distillation—A review”, *J. Membr. Sci.*, **475**, 215-244.
<https://doi.org/10.1016/j.memsci.2014.09.042>.
- Ullah, R., Khraisheh, M., Esteves, R.J., McLeskey Jr, J.T., AlGhouti, M., Gad-el-Hak, M. and Tafreshi, H.V. (2018), “Energy efficiency of direct contact membrane distillation”, *Desalination*, **433**, 56-67.
<https://doi.org/10.1016/j.desal.2018.01.025>.
- Usman, H.S., Touati, K. and Rahaman, M.S. (2021), “An economic evaluation of renewable energy-powered membrane distillation for desalination of brackish water”, *Renew. Energ.*, **169**, 1294-1304. <https://doi.org/10.1016/j.renene.2021.01.087>.
- Yang, C., Peng, X., Zhao, Y., Wang, X., Cheng, L., Wang, F., Li, Y. and Li, P. (2019), “Experimental study on VMD and its performance comparison with AGMD for treating copper-containing solution”, *Chem. Eng. Sci.*, **207**, 876-891.
<https://doi.org/10.1016/j.ces.2019.07.013>.
- Yuan, Z., Wei, L., Afroze, J. D., Goh, K., Chen, Y., Yu, Y., She, Q. and Chen, Y. (2019), “Pressure-retarded membrane distillation for low-grade heat recovery: The critical roles of pressure-induced membrane deformation”, *J. Membr. Sci.*, **579**, 90-101.
<https://doi.org/10.1016/j.memsci.2019.02.045>.
- Zhao, S., Liao, Z., Fane, A., Li, J., Tang, C., Zheng, C., Lin, J. and Kong, L. (2021), “Engineering antifouling reverse osmosis membranes: A review”, *Desalination*, **499**, 114857.
<https://doi.org/10.1016/j.desal.2020.114857>.